Seasonality of the meridional overturning circulation in the subpolar North Atlantic

Yao Fu, M. Susan Lozier, Tiago Carrilho Biló, Amy Bower, Stuart Cunningham, Frederic Cyr, Femke de Jong, Brad deYoung, Lewis Drysdale, Neil Fraser, Nora Fried, Heather H. Furey, Guoqi Han, Patricia Handmann, N. Penny Holliday, James Holte, Mark Inall, William E. Johns, Sam Jones, Johannes Karstensen, Feili Li, Astrid Pacini, Robert Pickart, Darren Rayner, Fiammetta Straneo, Igor Yashayaev

Abstract

Understanding the variability of the Atlantic Meridional Overturning Circulation on different timescales is essential for better predictions of our evolving climate. The newly updated time series (August 2014 to June 2020) from the Overturning in the Subpolar North Atlantic Program array allows us to examine the observation-based seasonality of the subpolar overturning, and meridional heat and freshwater transports for the first time. The overturning peaks in late spring and reaches a minimum in early winter, with a peak-to-trough range of 9.0 Sv. The overturning seasonal timing can be explained by winter transformation and the export of dense water, modulated by a seasonally-varying Ekman transport. Furthermore, over 55% of the total meridional freshwater transport variability can be explained by its seasonality, largely owing to overturning dynamics. Our results highlight the importance of seasonality in subpolar overturning variability and provide the first observational evidence of its variability on seasonal and longer timescales.

Introduction

Variability of the Atlantic Meridional Overturning Circulation (MOC) is broadly linked to climate variability because of its role in the global redistribution of heat and freshwater[1–3]. Despite numerous modeling studies linking MOC variability to changes in buoyancy forcing and subsequent water mass formation in the subpolar North Atlantic (SPNA)[4–6], observations of MOC variability in this region were lacking prior to 2014. To fill this need, the Overturning in the Subpolar North Atlantic Program (OSNAP) deployed an observing system in the summer of 2014 to continuously measure the subpolar meridional volume transport, i.e., MOC, as well as the trans-basin meridional heat and freshwater transports (MHT and MFT, respectively)[7,8].

The OSNAP array consists of two sections—OSNAP West, which runs from the coast of Labrador to West Greenland, and OSNAP East, which runs from East Greenland to the Scottish

shelf (Fig. 1). The array includes 60 moorings, 24 on the OSNAP West section focused near the basin boundaries off Labrador and west Greenland, and 36 along the OSNAP East section with highest density off East Greenland and over the Reykjanes Ridge. The first two years of OSNAP observations (2014-2016) showed that overturning in the eastern subpolar gyre (OSNAP East) dominated the mean and variability of the total subpolar MOC[8], challenging the conventional view that overturning in the Labrador Sea was a major contributor to the subpolar MOC. The updated four-year OSNAP time series (2014-2018) confirmed this result, and additionally showed that the variability in any one of the SPNA deep western boundary currents (DWBC) could capture only a small portion of the total MOC variability over the observational period[9]. For OSNAP East, density changes in the interior Irminger and Iceland basin rather than in the western boundary region appears to be important in explaining MOC variability. For OSNAP West, density anomalies in the Labrador Sea boundary currents compensate each other reducing overturning changes. These findings stand in contrast to the traditional interpretation that DWBC variability is closely linked to MOC lower limb variability[9].

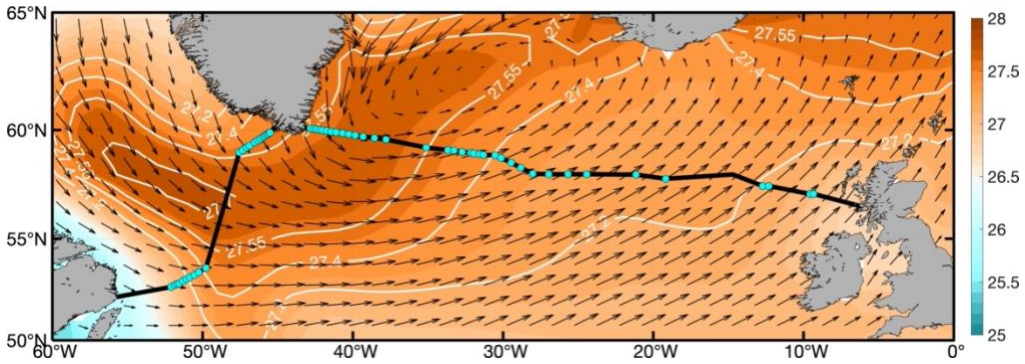

Figure 1 OSNAP Section. Winter (January to March) climatological wind stress from ERA5 (2014-2020) over the subpolar North Atlantic (vectors, in N m^{-2}) superimposed on climatological winter sea surface density from EN4 (shading with contours, in kg m^{-3}, for 2014-2020). OSNAP West and OSNAP East sections are indicated by black lines with OSNAP mooring positions denoted with cyan dots.

One of the most striking aspects of the OSNAP MOC, MHT, and MFT time series to date has been the strong variability shown by the observations, with a range of 15.0 Sv (1 Sv = 10^6 m^3 s^{-1}) in MOC (with a time mean of 16.6±0.7 Sv)[10], 0.2 PW in MHT (0.5±0.05 PW) and 0.2 Sv in MFT (0.36±0.05 Sv)[11]. The OSNAP time series used in the two prior analyses of MOC, MHT and MFT[8,10] were too short to ascertain the fraction of this variability that could be attributed to

seasonal forcing. With the six-year OSNAP record now in hand, a seasonal cycle of the subpolar MOC seems to be clearly emerging and is the focus of this paper.

Though the seasonality of the SPNA MOC, MHT and MFT have not previously been investigated with observations, several past studies provide useful guideposts for our study. For example, an idealized two-layer model with an interior and a boundary current was used[12] to link overturning variability in the Labrador Sea to wintertime dense water formation. This study linked a spring overturning peak to winter transformation and attributed the delay to the time required for dense water in the interior to be communicated to the boundary current. Such mechanism is also found to impact the Labrador overturning on interannual timescales based on a high-resolution (1/12°) ocean model[13]. Argo float data are used to investigate the overturning seasonal cycle in the Labrador Sea[14], which shows a maximum in spring and minimum in winter. For the eastern subpolar gyre, a recent study[15] revealed a fast export of newly formed Irminger Sea Intermediate Water (ISIW) into the OSNAP East boundary current off East Greenland. The newly formed waters reached the boundary current within one to three months after formation[15].

In addition to winter convection, wind forcing is also a likely cause of seasonality. Studies using data from RAPID (Rapid Climate Change-Meridional Overturning Circulation and Heatflux Array - Western Boundary Time Series) have shown that the seasonal cycle of the MOC in the tropical-subtropical Atlantic is largely driven by wind forcing via direct Ekman transport changes and isopycnal heaving at the eastern boundary[16–18]. By contrast, the climatological mean Ekman transport throughout the SPNA is weak. Over the first four years of OSNAP observation, the time-mean Ekman transport across the full OSNAP array is reported to be -1.5±0.2 Sv ("-" indicates southward), accounting for less than 10% of the time-mean MOC (16.6±0.7 Sv)[10]. Although the mean value is relatively small, Ekman transport might contribute substantially towards MOC variability, yet little attention has been paid to Ekman transport variability in this region. A recently submitted paper[19] shows that there is substantial seasonality in Ekman transports from -2Sv to -8Sv from the subpolar gyre interior into the boundary currents, which has the potential to impact MOC variability. As a first step to fill that gap, Ekman transport's imprint on MOC seasonality will be explored here.

Even less is known about the MHT and MFT seasonality in the SPNA. OSNAP observations to date indicate that overturning variability is primarily responsible for MHT and MFT variability[8,11], however, it is unclear how much of the MHT and MFT variability can be

explained by the corresponding seasonality. That determination is now possible with the new 71-month (about 6 years) OSNAP timeseries.

In summary, past analyses of the OSNAP time series have focused on the determination of the mean MOC and its variability, the partitioning of the MOC and associated meridional heat and freshwater transports between the two sections, and on the relationship between MOC variability and western boundary current variability. With this new 6-year time series, we focus on determining the MOC, MHT and MFT seasonality and investigate their relationship to wintertime transformation of water masses and wind-forced Ekman transport.

Results

The retrieval of mooring data in 2020 extended the OSNAP observation time series to 71 months, covering the period from August 2014 to June 2020 (Fig. 2). In the following, we first present the 6-year MOC time series, from which we determine MOC seasonality and explore how winter transformation and wind-driven Ekman transport impacts that variability. The 6-year MHT and MFT time series and their corresponding seasonality are then investigated.

MOC timeseries

Over the ~6 years of OSNAP observations, the MOC across the full OSNAP array exhibits strong monthly to interannual variability, with a range of 10-25 Sv and a standard deviation of 3.7 Sv. The mean MOC (± standard error) is 16.7±0.6 Sv. The standard error is estimated based on the effective number of degrees of freedom that takes into account autocorrelation of the time series (see Methods). As reported previously[8,10], the mean strength and variability of the MOC are dominated by overturning across OSNAP East (16.3±0.6 Sv, with a standard deviation of 2.9 Sv), rather than across OSNAP West (3.0±0.5 Sv, with a standard deviation of 1.5 Sv). The two new years in this time series (June 2018 to June 2020) reveal that the overturning at OSNAP East was relatively weak throughout 2019 and then rose sharply in the first half of 2020. Correspondingly, the MOC across the full array reached a maximum in May 2020 (26.4±4.6 Sv) with comparable strength of that in 2015 (25.6±4.8 Sv). The overturning at OSNAP West was relatively strong in both 2019 and 2020 compared to that in the first four years (Table S1). The mean OSNAP West MOC for the last two years (August 2018 -June 2020) is 3.9±0.9 Sv, substantially stronger than the first 2-year mean (2.5±0.6 Sv). The strongest monthly OSNAP West overturning, in May 2019, reaches 8.1±1.7 Sv and significantly contributes to the MOC peak across the full OSNAP array in that month.

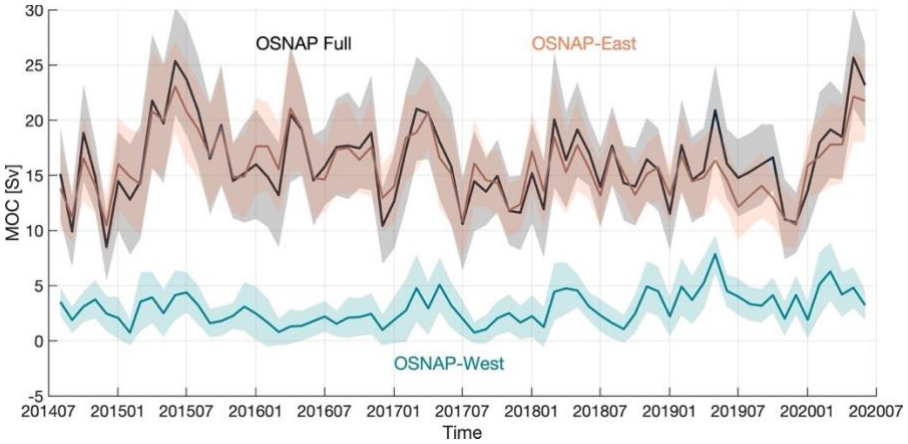

Figure 2 Meridional Overturning Circulation (MOC) time series. Monthly MOC timeseries across the full OSNAP array (black), OSNAP East (orange), and OSNAP West (cyan). Shading indicates monthly uncertainty estimated from a Monte Carlo analysis[8].

MOC seasonal cycle

A statistically significant seasonal cycle of the SPNA MOC is extracted by calculating the climatological mean MOC for each month using the 6-year OSNAP time series (Fig. 3a, see Methods). The seasonal MOC range for the full OSNAP section (maximum to minimum) is 8.8 Sv, with a maximum in spring (April to June) and a minimum in winter (December) (Table S2). Overall, seasonal variability explains about 40% of the total variability of the monthly MOC time series across the full OSNAP array over the 6-year observational period.

The MOC seasonal phase for OSNAP East and OSNAP West is similar to that across the full array (Fig. 3a). Consistent with other measures, seasonal variability of the full MOC is dominated by OSNAP East, with OSNAP West playing a lesser role. The range of the seasonal cycle is 6.2 Sv for OSNAP East and 2.6 Sv for OSNAP West, both with a maximum in May, but with the minimum at OSNAP West occurring in September rather than December for both OSNAP East and the full basin MOC. Overall, seasonality explains about 36% of the total variability of the monthly overturning at OSNAP East and about 25% at OSNAP West over the 6-year observational period. Note that neither the explained variability by the MOC seasonality at OSNAP East or West exceeds that across the full array. This can be explained by an enhanced MOC seasonality due to a combination of OSNAP East and OSNAP West MOC with their seasonality expressed over different periods. For instance, the OSNAP East MOC exhibits spring peaks over the observational period except in 2019, while the OSNAP West MOC only shows distinct seasonal cycle after 2017 (Fig. 2). Although the MOC across the full array is not a linear sum of the MOC across OSNAP

East and OSNAP West, the combination should still result in an enhanced MOC seasonality across the full array.

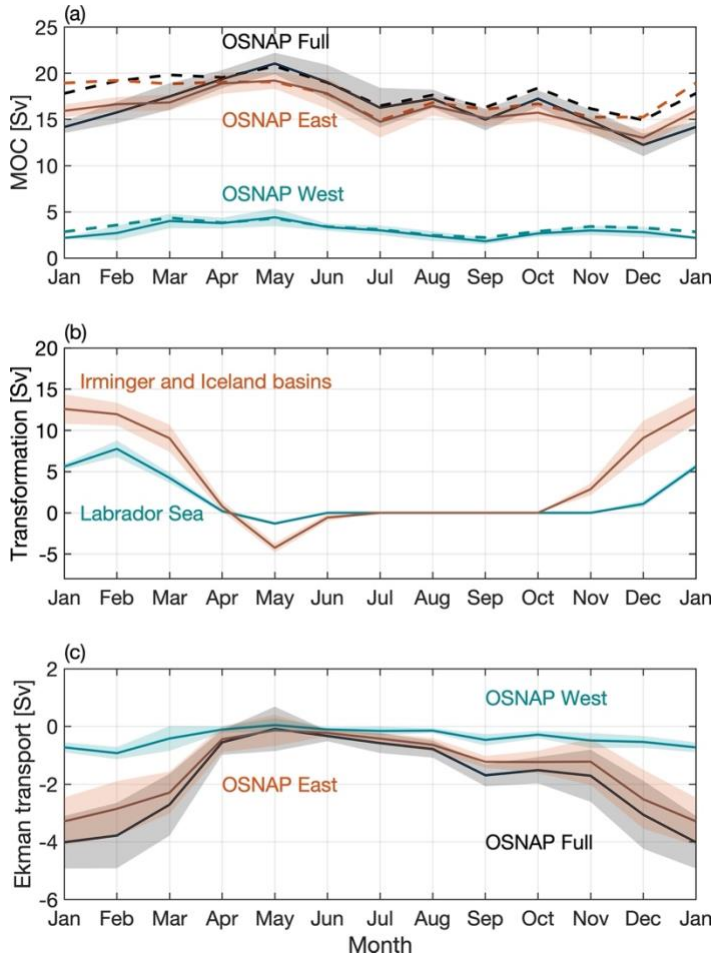

Figure 3 Seasonal cycle of the Meridional Overturning Circulation, transformation, and Ekman transport. Monthly climatology of (a) the MOC across the full OSNAP array (solid black), OSNAP East (solid orange), and OSNAP West (solid cyan), (b) transformation in the OSNAP East (orange) and OSNAP West (cyan) regions, and (c) Ekman transport across the full OSNAP array (black), OSNAP East (orange) and OSNAP West (cyan). The OSNAP West region is defined as the area between the 2000-m isobath of the Labrador Sea north of the OSNAP West line. The OSNAP East region is defined as the area between the OSNAP East section and the Greenland-Scotland-Ridge. Shading in the plots indicates the standard error of the monthly climatology over the 6-year OSNAP observation period. Ekman transport across the OSNAP array is calculated by projecting the total wind onto the OSNAP West and East sections. Dashed lines in (a) indicate the MOC seasonal cycle with both the Ekman transport and Ekman transport return flow removed (see Methods).

Wintertime transformation

North Atlantic Deep Water (NADW) is the primary source of the MOC lower limb. Therefore, the formation and southward transport of NADW in the SPNA has been linked to the

intensity and variability of the MOC[20]. To investigate the linkage between transformation and the MOC on seasonal timescales, we evaluate the seasonal cycle of water mass transformation (see Methods) across the 27.54 kg m^{-3} and 27.69 kg m^{-3} isopycnals in the eastern subpolar gyre (i.e., Irminger and Iceland basins) and western subpolar gyre (Labrador basin), respectively (Fig. 3b). Positive transformation indicates water of lighter density is converted to water of higher density due to air-sea heat and freshwater fluxes. The two isopycnals are the time-mean potential density surfaces of maximum overturning (σ_{MOC}) at OSNAP East and OSNAP West, respectively. Note that the MOC is calculated as the maximum of the overturning stream function, which occurs at different σ_{MOC} at different time steps. When transformation is calculated at time-varying σ_{MOC} for each month, the derived seasonality of transformation for both OSNAP East and OSNAP West region is qualitatively similar to that calculated at the time-mean σ_{MOC} (not shown). Transformation in both the eastern and western subpolar gyre shows a distinct peak in winter from December to March and remains near zero during the other months of the year, except in spring when re-stratification of the water column reduces surface water density leading to negative transformation (Fig. 3b).

Overturning across both OSNAP East and OSNAP West peaks in May which is 3 to 5 months after the maximum transformation, and then slowly declines over the rest of the year (Fig. 3a, solid lines). The OSNAP East overturning seasonality can be partly attributed to the fast export of ISIW (27.65 to 27.77 kg m^{-3}) by the East Greenland Current[15]. As previously reported, ISIW leaves the OSNAP East section within 1 to 3 months after formation off East Greenland[15], as evidenced by enhanced southward East Greenland Current transport from December to May (not shown)[10]. The spring overturning peak at OSNAP West matches the arrival of southward propagating density anomalies along the Labrador Sea western boundary at the OSNAP West array (Fig. S1). This timing is consistent with that predicted by Straneo et al. (2006) and highlights the expected importance of buoyancy forcing on seasonal timescales. In addition, the observed oxygen concentration in the LSW layer at OSNAP West also peaks in spring[21], consistent with the observed overturning maximum. The results above collectively indicate that wintertime formation and the export of dense water leads to increased overturning in winter at both OSNAP East and West.

The annual mean total production of lower layer water (with density larger than σ_{MOC}) via transformation is about 5.1±2.4 Sv (3.6±1.7 Sv in the Irminger and Iceland basin and 1.5±0.8 Sv

in the Labrador basin). The annual mean MOC across the full OSNAP array is 16.6±0.7 Sv. The difference of about 11.5 Sv between the MOC and transformation must be supplied by the overflow waters formed north of the Irminger and Iceland basins and via entrainment during the southward transport of the overflow waters. The Denmark Strait overflow is about 3.2±0.6 Sv[22], whose transport almost doubles downstream through entrainment. The Iceland-Scotland overflow Water transport at OSNAP East is approximately 5.3 Sv[23]. The sum of the two overflow water transports agrees well with the remaining transport reported above.

Ekman transport

We now assess the impact of Ekman transport (Eq. 3c) on MOC seasonal variability (see Methods). The 6-year mean Ekman transport (±standard error) across the full OSNAP array is southward, at -1.7±0.3 Sv, with the eastern subpolar gyre (OSNAP East) contributing -1.4±0.2 Sv to the total, and the western subpolar gyre (OSNAP West) contributing -0.4±0.1 Sv. These mean values are overshadowed by the large range of Ekman transports over its climatological seasonal cycle (Fig. 3c). Given that the westerly winds over the SPNA are strongest in winter and weakest in summer, we find the expected seasonality in Ekman transport. The monthly climatology of Ekman transport across the full array, always southward, has its maximum magnitude (-3.0 to -4.1 Sv) in winter (December to February) and its minimum (-0.1 to -0.3 Sv) in spring through summer (April to August) (Table S3).

The Ekman transport has a different impact on the two sections owing to their different orientation relative to the westerly winds: while the OSNAP East line is nominally zonal, OSNAP West is nearly orthogonal to the winds (Fig. 1). In addition, the OSNAP East section covers a much longer distance (~1970 km) than the OSNAP West section does (~890 km). As such, the impact of Ekman transport is pronounced for the OSNAP East overturning, yet of little consequence for the OSNAP West overturning. In particular, the seasonal cycle of Ekman transport enhances the overturning seasonal cycle at OSNAP East (and consequently across the full OSNAP array) by weakening the MOC in winter, when it opposes the generally northward flow of the upper ocean across the OSNAP line. In spring (May) the Ekman transport is nearly zero at both sections and has little impact on the MOC. As a result, the Ekman transport explains the timing of the MOC peak as well as 45% of the MOC magnitude (3.3 Sv) across the full array in winter (Fig. 3a, dashed lines, Table S2). Finally, we note that the seasonal impact of Ekman dynamics is insensitive to changes in the latitudinal position of OSNAP East of ± 1° (see Methods).

Summary of MOC seasonal variability

Overall, wintertime dense water formation and Ekman transport seasonality are two major contributors to MOC seasonal variability across the full OSNAP array. The wintertime dense water formation and export are responsible for the MOC peak in spring at both OSNAP East and OSNAP West, while the maximum southward Ekman transport in winter contributes significantly to the MOC minimum, which primarily applies to OSNAP East overturning, and thus to the full MOC.

An advantage of assessing the seasonal cycle is that its removal from the monthly MOC time series reveals the MOC interannual variability (Fig. S2). At OSNAP East, a strong MOC peak in 2015 is particularly evident, as are the weak MOC across OSNAP West in 2016 and the strong MOCs in 2019 and 2020 also across OSNAP West. An investigation on the mechanisms driving the SPNA MOC variability based on this OSNAP time series is underway.

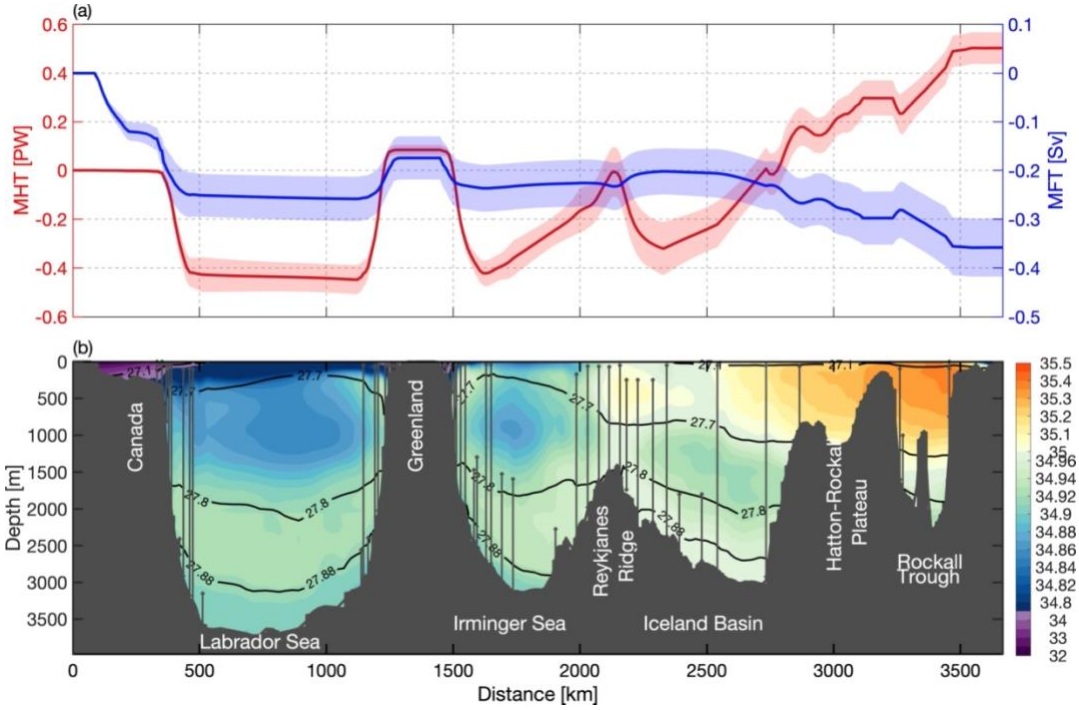

Figure 4 Salinity and meridional heat and freshwater transports across the OSNAP section. (a) Cumulative MHT (red) and MFT (blue) integrated from west to east. Northward transport is defined as positive. Shading indicates the corresponding standard deviation over the 6-year observational period. (b) The 6-year mean salinity section (colored shading) with moorings marked by the vertical black lines. The horizontal black lines represent the isopycnals of 27.10, 27.70, 27.80, and 27.88 kg m^{-3}.

Meridional heat and freshwater transports

Over the 6-year OSNAP observational period, the MHT has a mean (±standard error) of 0.50±0.01 PW. The eastern and western subpolar gyre contribute 0.42±0.01 PW and 0.08±0.01 PW, respectively, to this total. The heat transport across the section extending from the Iceland basin to the Scottish continental shelf dominates the total MHT (Fig. 4a, red), which is attributable to the northward transport of warm subtropical waters by the North Atlantic Current (NAC). The MHT exhibits strong monthly to interannual variability, which is clearly dominated by variability at OSNAP East (Fig. 5a). A decomposition of MHT into an overturning component and a gyre component[8] indicates that the overturning circulation accounts for 73% of the total subpolar MHT variability and the remaining part is attributed to gyre circulation. At OSNAP East, overturning dynamics explain ~ 90% of the MHT variability. At OSNAP West, overturning and gyre circulation dynamics each explains about 40% of the MHT variability.

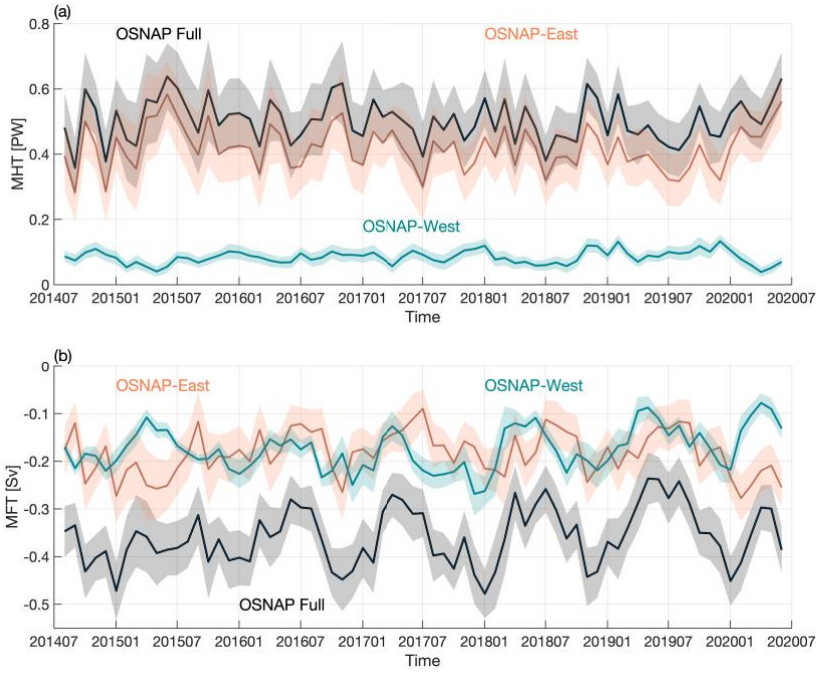

Figure 5 Meridional heat and freshwater transport time series. Monthly MHT (a) and MFT (b) across the full OSNAP array (black), OSNAP East (orange), and OSNAP West (cyan). Shading indicates the monthly uncertainty estimated using a Monte Carlo analysis[8].

The 6-year mean MFT (±standard error) across the full OSNAP array is -0.36±0.01 Sv. In contrast to the MOC and MHT, MFT across OSNAP West (-0.17±0.01 Sv) and OSNAP East (-0.18±0.01 Sv) contribute similarly to the total MFT with respect to both the mean and variability (Fig. 5b). This highlights the importance of the Labrador basin in terms of ocean freshwater transport, especially considering that the Labrador Sea has a smaller basin size and weaker

overturning compared to the eastern subpolar gyre[8]. The freshwater transport at OSNAP West is primarily concentrated in the Labrador Sea western boundary region (Fig. 4a, blue; see Methods), where the southward export of very fresh coastal waters (Fig. 4b) plays a significant role[11]. At OSNAP East, both the western boundary and NAC regions contribute to the southward freshwater transport, with the former related to the southward transport of fresh coastal waters, and the latter due to the northward transport of salty waters by the NAC, which is equivalent to a southward freshwater transport. The overturning component is responsible for ~ 53% of the subpolar MFT variability across the full OSNAP array, 66% across OSNAP East, and 87% across OSNAP West.

Seasonal variability of MHT

Compared to the MOC seasonality, MHT seasonality is relatively weak (Fig. 6). Across the full OSNAP array, the seasonal maximum to minimum MHT range of 0.10 PW is only 17% of the mean MHT, while the seasonal range of the MOC (~ 9.0 Sv) is ~ 50% of the mean. Only 21% of the total MHT variability across the full OSNAP array is explained by the seasonality, compared to (as mentioned above) 40% of the total MOC.

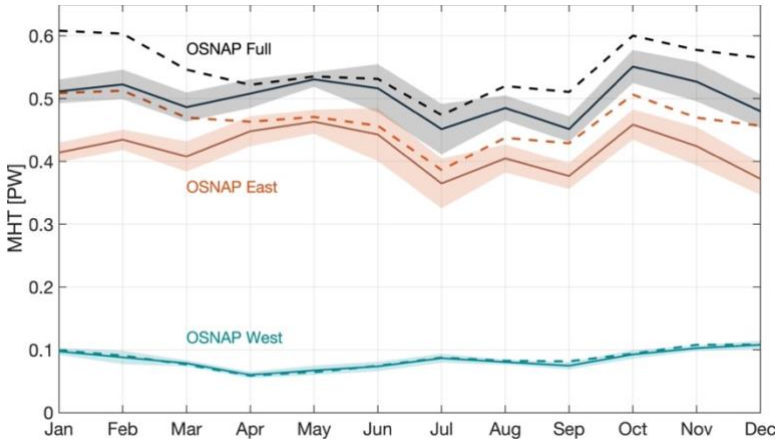

Figure 6 Seasonal cycle of meridional heat transport. MHT across the full OSNAP array (black), OSNAP East (orange), and OSNAP West (cyan). Shading shows the standard error of the monthly MHT climatology based on the 6-year OSNAP observation. Dashed lines indicate the MHT seasonal cycle after removal of the Ekman transport.

Seasonal MHT variability across the full OSNAP array mirrors that across OSNAP East. Both time series are marked by two maxima – one in spring and the other in autumn, and a minimum in summer (Fig. 6). MHT at OSNAP West, with a maximum in winter and minimum in spring, plays a minor role in seasonal MHT variability across the full array. Ekman transport at

OSNAP East, strongest in winter, carries relatively warm surface water southward, thus reducing the total northward MHT. As a result, the Ekman transport contribution to MHT greatly reduces the MHT seasonal variability at OSNAP East and across the full array, while it has little impact at OSNAP West (Fig. 6, dashed lines). The averaged difference of MHT from December to March due to Ekman transport contribution is about 0.08 PW for the full array and for OSNAP East.

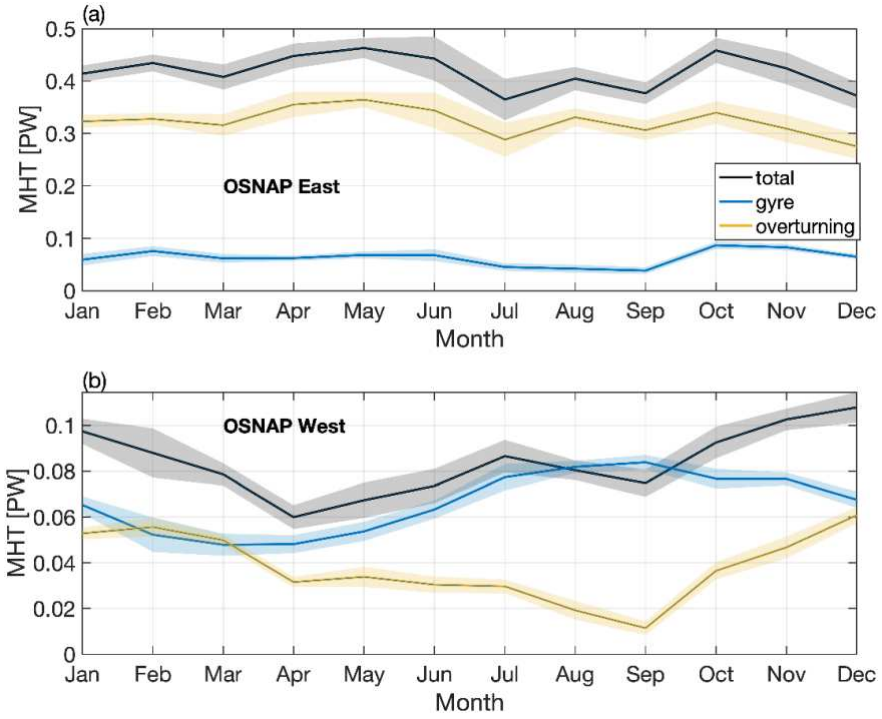

Figure 7 Decomposition of seasonal meridional heat transport. Decomposition of seasonal MHT at OSNAP East (a) and OSNAP West (b) into an overturning component (yellow) and a gyre component (blue). The total MHT is shown in black. Shading indicates standard error of the monthly climatology.

A decomposition of MHT variability into that due to overturning variability and that due to gyre variability explains the extrema noted above for OSNAP East and OSNAP West. The overturning contribution (inclusive of the Ekman contribution) is primarily responsible for MHT seasonal variability at OSNAP East (Fig. 7a), with a maximum northward heat transport in spring and minimum in winter. The maximum of MHT in spring is more muted than that of the MOC because the waters moving northward in the upper limb of the MOC are at their coldest point of the year in spring (March and April, not shown), offsetting the impact of increased overturning strength in spring. Similarly, the warmer upper ocean temperatures in late summer to early autumn (July to October) partially offset the reduction in the MOC at that time relative to spring, in terms

of the total MHT. The gyre contribution is relatively weak from January through September but strengthens in October and November due to an enhanced temperature difference between the western and eastern parts of the eastern subpolar basins in those months as well as enhanced gyre circulation in winter (Not shown). The enhanced gyre heat transport contributes to the second maximum of MHT across the full array in autumn. These two effects: the annual variation in upper limb average temperatures, and the gyre contribution to the MHT, largely explain why the MHT seasonal cycle is so much weaker than the MOC seasonal cycle.

At OSNAP West, both the overturning and gyre components contribute significantly to the mean and variability of MHT on seasonal timescales (Fig. 7b). Unlike OSNAP West MOC seasonal cycle, the overturning MHT component does not show a peak in spring, because the waters in the upper limb are coldest in early spring (March to April, not shown), reducing the northward heat transport by the MOC. The gyre component is weak in late winter and early spring (February to May) and strong in summer (July to September). This seasonal variation is largely attributed to the temperature contrast between the western and eastern half of the Labrador basin, which is strongest in summer and weakest in late winter and spring (Not shown).

Seasonal variability of MFT

Over 55% of the total MFT variability across the full OSNAP array can be explained by the seasonality over the observational period. The proportion even reaches 66% at OSNAP West, while it is about 37% at OSNAP East.

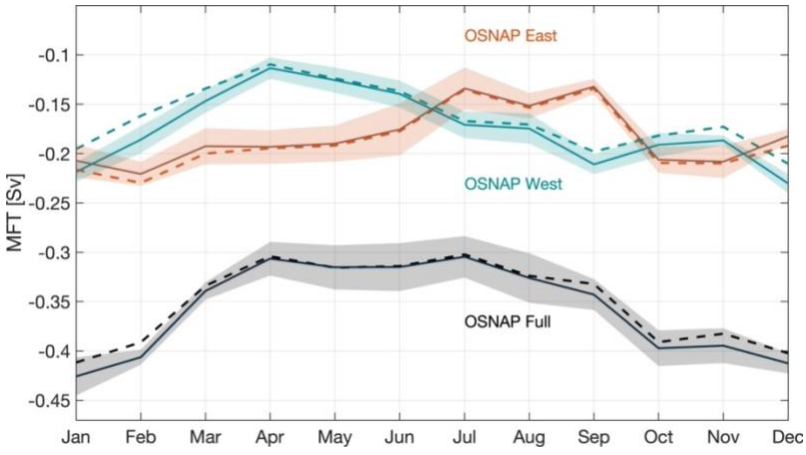

Figure 8 Seasonal cycle of meridional freshwater transport. MFT across the full OSNAP array (black), OSNAP East (orange), and OSNAP West (cyan). Shading indicates the standard error of the monthly MFT climatology based on the 6-year OSNAP observations. Dashed lines indicate MFT seasonal cycle after removal of the Ekman transport.

MFT across the full OSNAP array is strongest in winter and weakest in spring through summer (Fig. 8). Note that MFT is southward all year round. Here we refer to the strongest southward MFT as maximum, and weakest southward MFT as minimum. Distinct from the MOC and MHT, freshwater transport across both OSNAP East and OSNAP West contributes significantly to the MFT seasonal variability across the full OSNAP array. At OSNAP East, MFT is strongest from October to February, followed by a gradual decline until the summer minimum. At OSNAP West, the MFT seasonal time series has a pattern similar to that for MFT across the full array, with a maximum in winter and minimum in spring. The Ekman transport component has only a marginal impact on the MFT seasonality across the full array, OSNAP East and OSNAP West (Fig. 8, dashed lines). This is attributed to two factors: (1) the MFT seasonal cycle across the full array is more strongly expressed at OSNAP West, where the Ekman transport is weak throughout the year. (2) For OSNAP East, the section-mean salinity within the Ekman depth (about 25 m averaged over the section) over the OSNAP observation period is 35.01, close to the full-array mean salinity of 34.92 (see Methods). This penalizes the contribution of Ekman transport to MFT at OSNAP East.

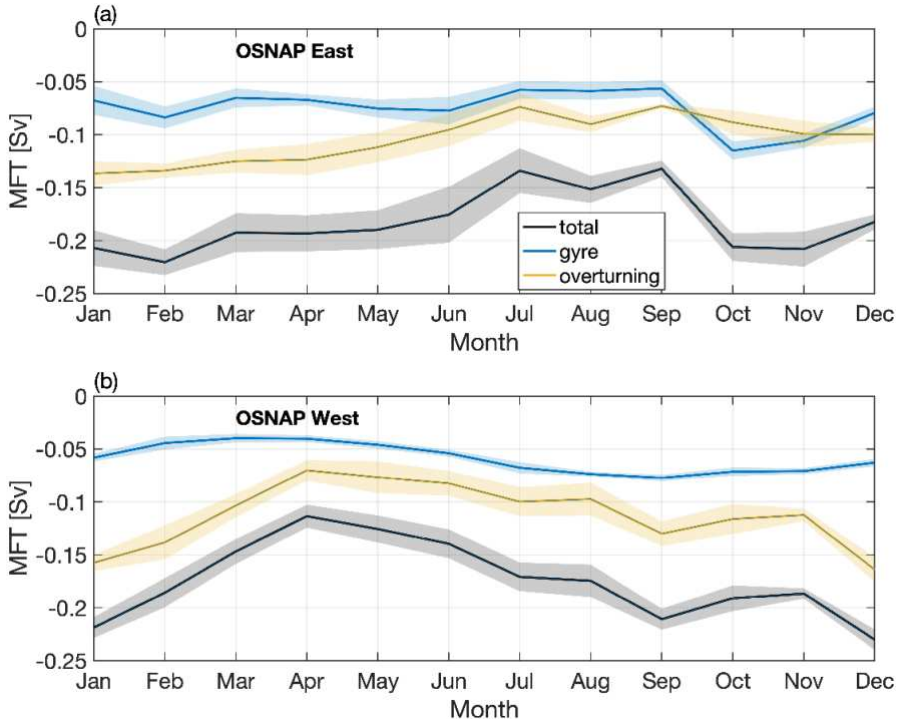

Figure 9 Decomposition of seasonal meridional freshwater transport. Decomposition of seasonal MFT at OSNAP East (a) and OSNAP West (b) into an overturning component (yellow) and a gyre component (blue). The total MFT is shown in black. Shading indicates standard error of the monthly climatology.

The decomposed MFT seasonal variability at OSNAP East reveals that the overturning component is primarily responsible for the total MFT seasonal variability, which decreases from a maximum in January to a minimum in July and then increases again from September to December (Fig. 9a). The seasonal cycle of the overturning component is dominated by freshwater export along the western boundary of the Irminger Sea and by a northward transport of salty waters in the NAC region, which both peak in winter months (not shown). Although the gyre circulation is strongest in winter, the gyre MFT component has an enhanced contribution in October and November, due to the highest zonal salinity contrast between the saline North Atlantic Water in the Iceland basin and Rockall Trough and the fresher water of coastal and Nordic Sea origin in the Irminger basin at that time.

At OSNAP West, the overturning component dominates the total MFT seasonal variability with a maximum in winter and a minimum in spring (Fig. 9b). The Labrador Sea western boundary plays a major role in the overturning component through the export of fresh coastal waters of Arctic origin out of the Labrador basin. The gyre component plays a secondary role with maximum southward freshwater transport in late summer and minimum in late winter and early spring owing to west-to-east salinity differences in the Labrador basin (not shown).

Summary

The extended 6-year OSNAP observations reveal robust seasonal variability of the MOC, MHT, and MFT in the SPNA, but particularly so for MOC and MFT for which seasonal variability accounts for a large fraction of the total variability. The MOC across both OSNAP East and OSNAP West peaks in spring and has a minimum in winter. This seasonality is largely driven by wintertime formation of dense water and its export and by the Ekman transport seasonal cycle. By reducing the northward transport in the upper layer primarily in winter, Ekman dynamics delay the appearance of the MOC peak, thus enhance the MOC seasonal cycle across OSNAP East and the full array.

During the 6-year OSNAP observational period (2014-2020), the winter North Atlantic Oscillation (NAO) was persistently in a positive phase. Because a positive NAO is associated with strong westerly winds and large heat loss over the subpolar regions[22], we suspect that our observations to date have captured a period during which the Ekman seasonality has a maximum

impact on the MOC. Our next two-year observational period will be telling since the NAO index was negative for the winter of 2021. Because the NAO has seasonal to decadal variability, we expect that Ekman dynamics will impact MOC variability on those same time scales. Wind variability is also expected to impact MOC variability through the generation of wind stress anomalies in the central and eastern SPNA that spawn baroclinic Rossby waves. These waves disturb isopycnals in their westward propagation[23], creating a baroclinic response of the velocity field on interannual timescales.

The MHT across the OSNAP array exhibits weak seasonal variability, due in large part to strong southward Ekman transport in winter, which offsets the northward flow of warm water in the MOC upper limb in the Iceland basin. This moderation of the MHT seasonal variability by the Ekman transport likely has implications for regional weather and ecosystems in the high-latitude North Atlantic region. Any moderating role for Ekman transport in the determination of MHT variability on longer timescales (i.e., interannual to decadal) is yet to be determined, but clearly of interest.

MFT's strong seasonal variability is primarily driven by the export of fresh and light coastal waters along the western boundary in the western subpolar gyre and is further amplified in winter and spring due to the enhanced transport of salty waters carried by the NAC. The dominance of the seasonal signal in the total MFT variability is largely expressed at OSNAP West. Though the Labrador Sea only weakly contributes to the MOC and MHT, this strong contribution to MFT highlights its potentially important role in future climate change. Studies have indicated that melt waters transported along the eastern boundary of the Labrador Sea contribute a significant portion of freshwater to the Labrador interior basin[26,27], the introduction of large amounts of freshwater from glacier melting into the subpolar basins poses an increased threat of a shutdown of deep convection[28]. As such, an understanding of how and where that freshwater input will have the largest impact on the MOC is crucial for improved predictions of climate variability and change.

Following on earlier published studies of the OSNAP time series[8,10], the current extension enhances our understanding of the SPNA overturning circulation. The seasonal variability of the MOC, MHT, and MFT explored in this study provides an observational basis for further studies on overturning variability and for model ground-truthing. With the ongoing OSNAP mooring turnaround in summer 2022, extending the time series to 8 years, an examination of the subpolar overturning variability on interannual to sub-decadal timescales will soon be possible. With a

likely weakening of the MOC in the coming decades[30], monitoring MOC variability and its connection to heat, freshwater, oxygen and carbon exports are vital for deepening our understanding of global climate variability.

Methods

MOC, MHT and MFT calculations

Following previous studies[8,10], the MOC is defined as the maximum of the overturning stream function, Ψ, in potential density (σ_θ) space as:

$$\mathrm{MOC}(t) = \max[\Psi(\sigma, t)] = \max\left[\int_{\sigma_{min}}^{\sigma_{max}} \int_{x_w}^{x_e} v(x, \sigma, t) dx d\sigma\right], \quad (1)$$

where v is the cross-sectional volume transport per unit length per unit density along the OSNAP section (positive poleward), which is integrated from west (x_w) to east (x_e) and from the smallest density surface (σ_{min}) to the largest (σ_{max}) throughout the water column. The density at which the overturning stream function reaches the maximum is σ_{MOC}. The MOC upper (lower) limb transport is the transport above (below) σ_{MOC} in the overturning stream function. The 2014-2020 mean σ_{MOC} is 27.63 kg m^{-3} across the full OSNAP section, 27.54 kg m^{-3} across OSNAP East, and 27.69 kg m^{-3} across OSNAP West.

MHT is defined as:

$$MHT(t) = \rho C_p \int_{\sigma_{min}}^{\sigma_{max}} \int_{x_w}^{x_e} v(x, \sigma, t) \theta(x, \sigma, t) dx d\sigma, \quad (2)$$

where ρ is potential density, C_p is the specific heat of seawater and θ is potential temperature.

MFT is defined as:

$$\mathrm{MFT}(t) = -\int_{\sigma_{min}}^{\sigma_{max}} \int_{x_w}^{x_e} v(x, \sigma, t) \frac{S(x, \sigma, t) - \bar{S}}{\bar{S}} dx d\sigma\,, \quad (3)$$

where S is salinity, and $\bar{S}$ is the area-weighted section mean salinity (34.92 for across the full OSNAP section).

Ekman transport calculation

The cross-sectional Ekman transport for the OSNAP section, M_{Ek}^{y}, is calculated from ERA5 surface wind stress as:

$$M_{Ek}^{y} = -\frac{1}{\rho_0}\frac{\tau_x}{f}, \qquad (4)$$

where ρ_0 is the density of sea water with a constant value of 1,025 kg m^{-3}, τ_x is the wind stress projected along the OSNAP section, and f is the Coriolis parameter. The Ekman transport is applied to the OSNAP section where there is no direct velocity measurement near the surface[8] and within the theoretical Ekman layer[31]. The section-mean Ekman layer depth is about ~25 m.

The zero net volume transport constraint across the full OSNAP section requires the surface-layer Ekman transport to be balanced by an instantaneous barotropic return flow that is evenly distributed across the full section. In the calculation of the MOC, MHT and MFT without Ekman transport components, we removed the Ekman transport in the Ekman layer and the Ekman return flow from the derived velocity field at each time step.

Ekman transport across OSNAP East dominates the mean and variability of the total Ekman transport across the full array. This dominance can be attributed to the fact that the orientation of the OSNAP East section is almost parallel to the westerly winds, which generates large cross-sectional Ekman transport. To test the sensitivity of the Ekman transport strength to the latitudinal location of the OSNAP East, we randomly shifted the entire OSNAP East section within 1° latitude to the north or south of its current position. These runs yielded mean Ekman transports within 0.1 Sv of the mean Ekman transport (-1.7±0.3 Sv) across the current line, leading us to conclude that sensitivity to local latitudinal variability is weak.

Water mass transformation rate

Following previous studies[20,32], the rate of water mass transformation, F, is calculated by integrating surface density fluxes induced by air-sea buoyancy fluxes over the outcropping area of a given isopycnal as:

$$F(\sigma^*) = \frac{1}{\Delta\sigma}\iint\left[-\frac{\alpha}{C_p}Q + \beta\frac{S}{1-S}(E-P)\right]\prod\sigma\, dxdy, \qquad (5)$$

where

$$\prod\sigma = \begin{cases} 1 & \text{for } [\sigma-\sigma^*] \leq \frac{\Delta\sigma}{2} \\ 0 & \text{elsewhere.} \end{cases}$$

In Eq. (5), α and β are the thermal expansion and haline contraction coefficients, respectively. Q is the net heat flux into the ocean, and S is the surface salinity. E and P are the evaporation and precipitation rates, respectively. $\Delta\sigma = 0.2$ kg m^{-3} is the density bin size that the

outcropping density (σ^*) represents. Positive transformation indicates conversion of water lighter than the specified isopycnal to water denser than the isopycnal. The Labrador basin is defined as the area enclosed by the 2000-m isobath of the Labrador Sea and the OSNAP West line. Using the 2000-m isobath excludes the shallow continental shelf region (water depth smaller than 300 m) along the Labrador coast, where water is much lighter than mean σ_{MOC} of 27.69 kg m^{-3} in the Labrador Sea. The continental slope on both sides of Greenland is very steep. Using the coastline or 2000-m isobath has negligible impact on the outcropping area. The eastern subpolar gyre is defined as the area between the OSNAP East section and the Greenland-Scotland-Ridge[20].

The National Centers for Environmental Prediction Climate Forecast System v2 (NCEP/CFSv2) heat and freshwater fluxes and Roemmich-Gilson Argo Climatology monthly temperature and salinity from January 2014 to December 2020 are used to calculate the transformation. Using a different combination of datasets, for example, NCEP/CFSv2 heat and freshwater fluxes with surface temperature and salinity derived from the Met Office EN4, results in a qualitatively similar transformation seasonal cycle, with the same phase yet a slightly different winter transformation. Specifically, the December-to-March mean transformation (±standard deviation) for the eastern subpolar gyre is 10.7±1.9 Sv and 11.8±1.8 Sv for the Argo-based and EN4-based calculations, respectively. The values for the western subpolar gyre are 4.6±2.8 Sv and 4.3±1.9 Sv for the Argo-based and EN4-based calculations, respectively. Given the similarity of these estimates, we use the combination of NCEP/CFSv2 and Argo to demonstrate the seasonal cycle of water mass transformation.

Monthly climatology calculation

The climatological mean MOC, MHT and MFT for each month from January to December are calculated based on the 71-month OSNAP observations that cover the period from August 2014 to June 2020. For January to June and August to December, there are 6 monthly realizations during the 71-month observational period. For July, there are only 5 monthly values during the same period. The monthly climatology is calculated by averaging the available realizations of each month. The standard error of the monthly climatological mean is used as the uncertainty and is calculated as the standard deviation divided by the square root of the number of available realizations of each month (i.e., 5 for July and 6 for the other months).

Uncertainty estimates for the time-mean MOC, MHT and MFT

The standard error of the 71-month mean MOC, MHT and MFT is used as the uncertainty of the time-mean values. The standard error is calculated as:

$$SE = \frac{STD}{\sqrt{DOF}}, \qquad (6)$$

where STD represents the standard deviation of a quantity (i.e., the MOC, MHT and MFT) based on the corresponding monthly time series. DOF is the effective number of degrees of freedom, which is calculated as the total length of a time series divided by the decorrelation timescale. The decorrelation timescale is determined as the integral of the corresponding autocorrelation function between the first positive and negative zero-crossings[33]. We estimate that there are 43, 30 and 13 independent values in the 71-month MOC time series for the full array, OSNAP East, and OSNAP West, respectively.

MOC calculation updates

Several updates have been implemented in the MOC calculations since Li et al.[10] with respect to the configuration of the OSNAP array (i.e., adding or removing moorings), averaging window of the time series, and recalibration of instruments. These updates impact the calculation of the cross-sectional velocity field, which marginally changes the MOC that is calculated based on the cross-sectional velocity (Eq. 1). Here we document each change and evaluate the impact of this change on the MOC by comparing the MOC estimates with and without this specific change.

Averaging window. In the previous OSNAP calculations, the MOC is calculated using 30-day averaged mooring and auxiliary data (e.g., Argo temperature and salinity profiles, wind, sea surface height, etc.)[8,10], resulting in a MOC time series with 30-day temporal resolution. As the OSNAP observations have been extended to ~6 years and will continue to a longer period, the 30-day averaging window will, in time, lead to a growing misalignment between the 30-day time series and the calendar months. Therefore, from this study onward, the MOC is calculated using monthly-averaged mooring and auxiliary data to obtain an OSNAP time series aligned with calendar months, currently from August 2014 to June 2020. Since the MOC time series is calculated based on either monthly-averaged or 30-day-averaged mooring and auxiliary data, a negligible difference of 0.02 Sv is detected in the 6-year mean for the full OSNAP array. However,

when the monthly and 30-day MOC time series are derived from the same daily MOC time series, they have an identical time-mean value.

Ekman transport calculation. In the previous OSNAP metrics calculation[10], the Ekman transport across the full OSNAP section is calculated using wind stress derived from European Centre for Medium-Range Weather Forecasts (ECMWF) ERA5 wind speed using a bulk formula[34]. Since ERA5 directly provides wind stress data, the Ekman transport is directly calculated using the ERA5 wind stress from this study onward. Compared to the previous calculation, using the ERA5 wind stress decreased mean MOC across the full array by only 0.06 Sv, which is much smaller than the uncertainty range.

Inclusion of the data from moorings LSA and LSB on the West Greenland shelf. Two additional moorings, LSA and LSB, were deployed in September of 2018 at the eastern end of the OSNAP West line to measure the inshore West Greenland Coastal Current and its water properties. The West Greenland Coastal Current carries the freshest coastal water northward into the Labrador Sea along the eastern coast. The two moorings continuously measure current velocity, temperature and salinity throughout the water column of ~ 120 m. Including the two moorings in the calculation results in an increase of the full MOC by ~ 0.2 Sv and a decrease of southward MFT by ~ 0.01 Sv.

Removal of M5 mooring in the central Irminger Sea. M5 was a deep mooring located near the center of the Irminger Sea along the OSNAP East line. It was deployed to cover the water column from 1500 m to the sea floor from August 2014 to June 2018. In the mean, M5 captured a northward velocity over its deployment period. In order to assess the impact of M5's removal, a comparison between the MOC estimates with and without the data from M5 for the deployment period was performed. The result indicates that removing M5 in the calculation leads to a strengthening of the mean MOC by 0.4 Sv. Our interpretation is that M5 measured a northward recirculation branch in the MOC lower limb that reduced the MOC estimate. For consistency with the first 4-year OSNAP calculation, we use the data from M5 in the MOC calculation from August 2014 to June 2018. After June 2018, no M5 data are available. Geostrophic velocity determined using mooring data on both sides of the original M5 position is used to fill the vacancy of M5.

Using directly measured velocity from moorings D1, D2 and D3 along the eastern flank of the Reykjanes Ridge. Moorings D1, D2 and D3 are located on the eastern flank of the Reykjanes Ridge in the Iceland Basin. Prior to 2018 they were configured for velocity and property measurements below 1200 m only. Velocity above 1200 m over the three moorings was calculated from geopotential height data provided by two tall moorings, one to the west and the other to the east[35]. Starting in July 2018, the three moorings were extended to cover the entire water column, allowing for the use of direct velocity measurements in the MOC calculation. A comparison of the MOC estimates for July 2018 - June 2020 using geostrophic velocities with those using direct velocities shows that the latter results in a larger total MOC of just ~ 0.1 Sv. The MOC variability is similar for the two cases. This good agreement validates the application of end-point geostrophy over this region for the MOC estimate over the 2014-2018 period.

IB5 mooring replaced glider measurement over the Hatton-Rockall Basin. An additional mooring, IB5, was newly installed on the Hatton Bank along the OSNAP East section in July 2018. This mooring was added as a replacement for the discontinued glider observations with the last measurement in the Hatton-Rockall Basin in December 2017. IB5 is designed to capture the branch of the NAC in the Hatton-Rockall basin with velocity and property measurements. A comparison between the MOC calculation with and without the IB5 data shows that its inclusion increases the mean MOC by ~ 0.5 Sv for the period from July 2018 to June 2020. A comparison of the MOC estimates with and without the glider data during the 2014-2017 period shows that including the glider data also increases the MOC by ~0.5 Sv. In light of the agreement between these two comparisons, we conclude that IB5 has adequately substituted for the glider measurements in the OSNAP observing system.

Recalibration of the 53°N array along the Labrador Sea western boundary and moorings M1, M2 and M3 along the Irminger Sea western boundary. A bias in the salinity data from the 53°N array at OSNAP West and in the Deep Western boundary moorings M1, M2 and M3 at OSNAP East for the period of August 2016 to June 2018 has been attributed to calibration error of the salinometer on board the cruise MSM74. MSM74 was responsible for the recovery and deployment of the moorings mentioned above in May and June 2018. To correct the bias in the mooring data, all affected salinities were increased by 0.004. This recalibration of the salinity data

has only a minimum impact on the MOC. For both OSNAP East and OSNAP West, the difference in the mean MOC for the affected period is less than 0.1 Sv, much smaller than the uncertainties in the means.

Labrador Shelf measurements. As previously reported Labrador shelf is an unmeasured component in the OSNAP calculation[10] with velocity and property fields estimated based on monthly climatology from multi-model ensemble and World Ocean Atlas 2018, respectively. The long-term (1950 to 2016) mean freshwater transport on the Labrador shelf is estimated to be about 0.06 Sv[27], accounting for more than 30% of the OSNAP West freshwater transport. To understand the impact of freshwater transport in this region on the total subpolar freshwater transport variability, two additional moorings measuring the Labrador coastal and shelf-break currents have been deployed since the summer 2020 and four new moorings are planned to be deployed in 2023 within 100 km from the Labrador coast.

Data availability

The 2014-2020 OSNAP MOC time series and derived velocity, temperature, and salinity fields are available in SMARTech Repository. The calibration and quality-control of the moored instrument and glider data are performed by each participating group and are available at www.o-snap.org. The Argo climatology is available at http://sio-argo.ucsd.edu/RG_Climatology.html. The ECMWF ERA5 wind data are available at https://cds.climate.copernicus.eu/. The Met Office EN4 data are available at https://www.metoffice.gov.uk/hadobs/en4/. The NCEP surface heat and freshwater fluxes are available at https://rda.ucar.edu/datasets/ds094.0/.

Code availability

The calculation code for OSNAP metrics is available in SMARTech Repository. Detailed information about the code is upon request to YF.

Reference

1. Buckley, M. W. & Marshall, J. Observations, inferences, and mechanisms of the Atlantic Meridional Overturning Circulation variability: A review. *Rev. Geophys.* **54**, 5–63 (2016).
2. Knight, J. R., Folland, C. K. & Scaife, A. A. Climate impacts of the Atlantic multidecadal oscillation. *Geophys. Res. Lett.* **33**, 2–5 (2006).

3. Yeager, S. G., Karspeck, A., Danabasoglu, G., Tribbia, J. & Teng, H. A decadal prediction case study: Late twentieth-century north Atlantic Ocean heat content. *J. Clim.* **25**, 5173–5189 (2012).
4. Yeager, S. *et al.* An outsized role for the Labrador Sea in the multidecadal variability of the Atlantic overturning circulation. *Sci. Adv.* **7**, 1–25 (2021).
5. Thornalley, D. J. R. *et al.* Anomalously weak Labrador Sea convection and Atlantic overturning during the past 150 years. *Nature* **556**, 227–230 (2018).
6. Jackson, L. C., Peterson, K. A., Roberts, C. D. & Wood, R. A. Recent slowing of Atlantic overturning circulation as a recovery from earlier strengthening. *Nat. Geosci.* **9**, 518–522 (2016).
7. Lozier, M. S. *et al.* Overturning in the Subpolar north Atlantic program: A new international ocean observing system. *Bull. Am. Meteorol. Soc.* **98**, 737–752 (2017).
8. Lozier, M. S. *et al.* A sea change in our view of overturning in the subpolar North Atlantic. *Science (80-.).* **363**, 516–521 (2019).
9. McCartney, M. S. Recirculating components to the deep boundary current of the northern North Atlantic. *Prog. Oceanogr.* **29**, 283–383 (1992).
10. Li, F. *et al.* Subpolar North Atlantic western boundary density anomalies and the Meridional Overturning Circulation. *Nat. Commun.* **12**, 1–9 (2021).
11. Li, F. *et al.* Observation-based estimates of heat and freshwater exchanges from the subtropical North Atlantic to the Arctic. *Prog. Oceanogr.* **197**, 102640 (2021).
12. Straneo, F. On the connection between dense water formation, overturning, and poleward heat transport in a convective basin. *J. Phys. Oceanogr.* **36**, 1822–1840 (2006).
13. Feucher, C., Garcia-Quintana, Y., Yashayaev, I., Hu, X. & Myers, P. G. Labrador Sea Water Formation Rate and Its Impact on the Local Meridional Overturning Circulation. *J. Geophys. Res. Ocean.* **124**, 5654–5670 (2019).
14. Holte, J. & Straneo, F. Seasonal Overturning of the Labrador Sea as Observed by Argo Floats. *J. Phys. Oceanogr.* **47**, 2531–2543 (2017).
15. Le Bras, I. A. -A., Straneo, F., Holte, J., Jong, M. F. & Holliday, N. P. Rapid Export of Waters Formed by Convection Near the Irminger Sea's Western Boundary. *Geophys. Res. Lett.* **47**, (2020).
16. Zhao, J. & Johns, W. Wind-driven seasonal cycle of the atlantic meridional overturning circulation. *J. Phys. Oceanogr.* **44**, 1541–1562 (2014).
17. Kanzow, T. *et al.* Seasonal Variability of the Atlantic Meridional Overturning Circulation at 26.5°N. *J. Clim.* **23**, 5678–5698 (2010).
18. Zhao, J. & Johns, W. E. Wind-forced interannual variability of the Atlantic Meridional Overturning Circulation at 26.5°N. *J. Geophys. Res. Ocean.* **119**, 2403–2419 (2014).
19. Jones, S. C., Fraser, N. J., Cunningham, S. A., Fox, A. D. & Inall, M. E. Observation-based estimates of volume , heat and freshwater exchanges between the subpolar North Atlantic interior, its boundary currents and the atmosphere. *EGUsphere* **2022**, 1–38 (2022).
20. Petit, T., Lozier, M. S., Josey, S. A. & Cunningham, S. A. Atlantic Deep Water Formation Occurs Primarily in the Iceland Basin and Irminger Sea by Local Buoyancy Forcing. *Geophys. Res. Lett.* **47**, 1–9 (2020).
21. Koelling, J., Atamanchuk, D., Karstensen, J., Handmann, P. & Wallace, D. W. R. Oxygen export to the deep ocean following Labrador Sea Water formation. *Biogeosciences* **19**, 437–454 (2022).

22. Jochumsen, K. *et al.* Revised transport estimates of the Denmark Strait overflow. *J. Geophys. Res. Ocean.* **122**, 3434–3450 (2017).
23. Johns, W. E., Devana, M., Houk, A. & Zou, S. Moored Observations of the Iceland-Scotland Overflow Plume Along the Eastern Flank of the Reykjanes Ridge. *J. Geophys. Res. Ocean.* **126**, 1–26 (2021).
24. Greatbatch, R. J. The North Atlantic Oscillation. *Stoch. Environ. Res. Risk Assess.* **14**, 0213–0242 (2000).
25. Wang, H., Li, Z., Lin, X., Zhao, J. & Wu, D. Adiabatic Processes Contribute to the Rapid Warming of Subpolar North Atlantic During 1993–2010. *J. Geophys. Res. Ocean.* **127**, 1–16 (2022).
26. Böning, C. W., Behrens, E., Biastoch, A., Getzlaff, K. & Bamber, J. L. Emerging impact of Greenland meltwater on deepwater formation in the North Atlantic Ocean. *Nat. Geosci.* **9**, 523–527 (2016).
27. Schulze Chretien, L. M. & Frajka-Williams, E. Wind-driven transport of fresh shelf water into the upper 30m of the Labrador Sea. *Ocean Sci.* **14**, 1247–1264 (2018).
28. Oltmanns, M., Karstensen, J. & Fischer, J. Increased risk of a shutdown of ocean convection posed by warm North Atlantic summers. *Nat. Clim. Chang.* **8**, 300–304 (2018).
29. Florindo-López, C. *et al.* Arctic ocean and hudson bay freshwater exports: New estimates from seven decades of hydrographic surveys on the Labrador shelf. *J. Clim.* **33**, 8849–8868 (2020).
30. Collins, M. *et al.* Extremes, Abrupt Changes and Managing Risks. *IPCC Spec. Rep. Ocean Cryosph. a Chang. Clim.* 589–655 (2019).
31. Ekman, V. W. On the influence of the earth's rotation on ocean-currents. *Astron. Phys.* **2**, (1905).
32. Speer, K. & Tziperman, E. Rates of Water Mass Formation in the North Atlantic Ocean. *Journal of Physical Oceanography* vol. 22 93–104 (1992).
33. Cunningham, S. A. *et al.* Temporal Variability of the Atlantic Meridional Overturning Circulation at 26.5 N. *Science (80-.).* **317**, 935–938 (2007).
34. Large, W. G. & Pond, S. Open Ocean Momentum Flux Measurements in Moderate to Strong Winds. *J. Phys. Oceanogr.* **11**, 324–336 (1981).
35. Li, F., Lozier, M. S. & Johns, W. E. Calculating the meridional volume, heat, and freshwater transports from an observing system in the subpolar North Atlantic: Observing system simulation experiment. *J. Atmos. Ocean. Technol.* **34**, 1483–1500 (2017).
36. Yashayaev, I. & Loder, J. W. Further intensification of deep convection in the Labrador Sea in 2016. *Geophys. Res. Lett.* **44**, 1429–1438 (2017).
37. Li, F. & Lozier, M. S. On the linkage between Labrador Sea Water volume and overturning circulation in the Labrador Sea: A case study on proxies. *J. Clim.* **31**, 5225–5241 (2018).

Supplementary figures

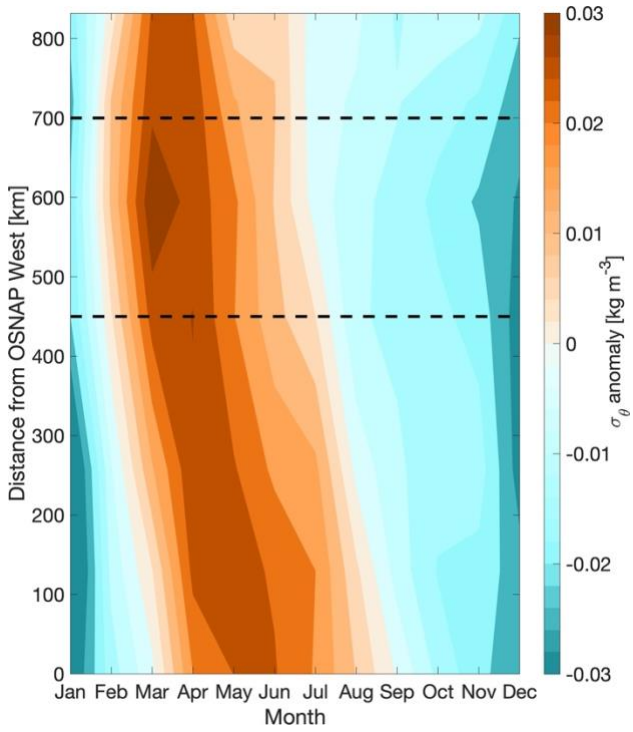

Figure S1 Seasonal propagation of potential density anomaly along the Labrador Sea western boundary. Potential density between 200 and 400 m, calculated using Roemmich-Gilson gridded Argo data, is horizontally averaged within 2°×1° (longitude×latitude) bins centered on the 2500-m isobath. Potential density anomaly is calculated by subtracting the mean potential density of each bin. The 200-400 m range covers the depth range of the time-mean σ_{MOC} (27.69 kg m^{-3}) at OSNAP West, which has a mean depth of about 270 m along the western boundary. Y-axis represents the distance northward from OSNAP West. The two black dashed lines, one at 700 km and the other at 450 km, represent the approximate positions of 58°N and the AR7W hydrographic section (55°N) along the western boundary, respectively, which bracket the core of the climatological convection region in the Labrador Sea[36,37].

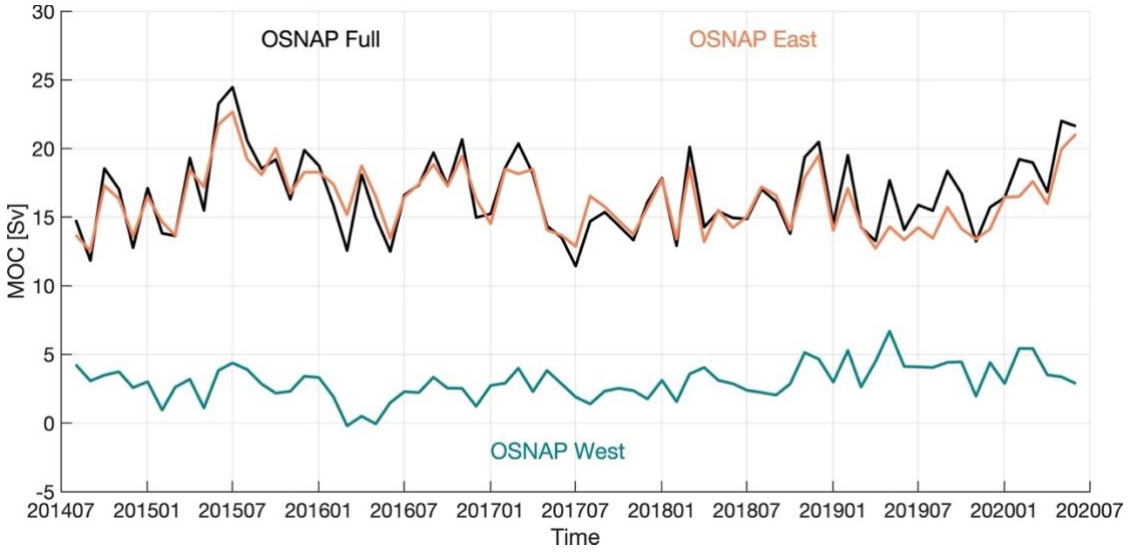

Figure S2 Monthly MOC time series with the seasonal cycle removed. The climatological monthly anomaly derived from the 6-year OSNAP observations is removed from the original OSNAP MOC time series across the full OSNAP array (black), OSNAP East (orange), and OSNAP West (cyan).

Table S1 Annual mean MOC across the OSNAP full array, OSNAP East and OSNAP West. The annual mean values are calculated from August to July of the next year. Note that the last available monthly value is in June 2020. Therefore, the values in the last column are derived based on 11 months observation from August 2019 to June 2020. The annual mean and standard error of the mean are derived based on the monthly values within the corresponding annual period. The corresponding standard deviation is shown in parenthesis.

Section	Aug 2014-Jul 2015	Aug 2015-Jul 2016	Aug 2016-Jul 2017	Aug 2017-Jul 2018	Aug 2018-Jul 2019	Aug 2019-Jun 2020
Full array	16.8±2.1 (5.4)	17.0±1.0 (2.6)	16.8±1.4 (3.5)	15.3±1.2 (3.0)	16.3±1.0 (2.5)	17.7±1.9 (4.7)
OSNAP East	16.5±2.0 (4.0)	17.3±1.1 (2.3)	16.6±1.4 (2.7)	15.3±1.2 (2.3)	15.4±0.8 (1.6)	16.3±2.0 (4.0)
OSNAP West	3.0±1.0 (1.1)	2.0±0.7 (0.8)	2.7±1.2 (1.3)	2.6±1.3 (1.4)	3.9±1.8 (2.0)	3.9±1.2 (1.3)

Table S2 Climatological monthly MOC over the 6-year OSNAP observations. The climatological monthly mean and the standard error is provided for each month across the full OSNAP array, OSNAP East and OSNAP West. The value in parenthesis indicates the climatological monthly MOC with the Ekman transport component removed. Note that both the Ekman transport and the Ekman return flow are removed (see Methods).

Section	Jan	Feb	Mar	Apr	May	Jun	Jul	Aug	Sep	Oct	Nov	Dec
Full array	14.2±0.6 (17.8±1.1)	15.8±1.2 (19.2±1.0)	17.5±1.4 (19.8±1.1)	19.4±1.0 (19.6±1.4)	21.1±1.2 (20.8±1.2)	19.0±1.9 (19.0±1.9)	16.3±2.1 (16.5±1.9)	17.2±1.0 (17.6±1.1)	15.0±1.2 (16.3±1.0)	17.3±0.9 (18.4±0.7)	14.8±1.2 (16.2±1.3)	12.3±1.2 (14.9±0.9)
OSNAP East	15.9±0.7 (18.9±1.1)	16.7±0.8 (19.2±0.8)	16.8±0.9 (18.9±0.5)	18.9±1.1 (19.1±1.5)	19.2±0.9 (19.1±1.2)	17.8±1.6 (17.8±1.7)	14.7±1.7 (14.9±1.6)	16.5±1.0 (16.8±1.6)	15.2±0.9 (16.1±0.8)	15.7±1.0 (16.7±1.0)	14.3±1.0 (15.3±1.3)	13.0±0.9 (15.3±0.9)
OSNAP West	2.2±0.1 (2.8±0.2)	2.7±0.8 (3.6±0.8)	4.0±0.8 (4.4±0.7)	3.8±0.6 (3.8±0.5)	4.4±1.0 (4.3±0.8)	3.3±0.4 (3.4±0.4)	3.0±0.5 (3.1±0.4)	2.4±0.5 (2.5±0.5)	1.8±0.3 (2.2±0.3)	2.7±0.3 (2.9±0.3)	3.0±0.5 (3.4±0.4)	2.8±0.6 (3.3±0.5)

Table S3 Climatological monthly Ekman transport over the 6-year OSNAP observations. The climatological monthly mean and standard error are provided for each month across the full OSNAP array, OSNAP East and OSNAP West.

Section	Jan	Feb	Mar	Apr	May	Jun	Jul	Aug	Sep	Oct	Nov	Dec
Full array	-4.0±0.9	-3.8±1.1	-2.7±1.1	-0.5±0.4	-0.1±0.8	-0.3±0.2	-0.6±0.3	-0.8±0.3	-1.7±0.4	-1.5±0.5	-1.7±0.9	-3.0±1.2
OSNAP East	-3.3±0.8	-2.9±0.9	-2.3±0.7	-0.4±0.4	-0.1±0.5	-0.2±0.1	-0.4±0.2	-0.6±0.2	-1.2±0.2	-1.2±0.4	-1.2±0.8	-2.5±1.0
OSNAP West	-0.7±0.2	-0.9±0.2	-0.4±0.4	-0.1±0.1	0.0±0.2	-0.1±0.1	-0.2±0.2	-0.1±0.1	-0.5±0.2	-0.3±0.1	-0.5±0.3	-0.5±0.2